Chinese Journal of Natural Medicines

**Huatuo Zaizao Pills improve myocardial ischemia by inhibiting extracellular calcium influx**

Nannan Wang, Shifeng Cao, Yu Zhao, Yanrong Li, Jiewen Zhou, Shuyu Liu, Huan Chen, Na An, Linhe Liu, Yixiu Zhao, Hongxia Zhao, Na Ning, Yan Zhang, Baofeng Yang

**Citation:** Nannan Wang, Shifeng Cao, Yu Zhao, Yanrong Li, Jiewen Zhou, Shuyu Liu, Huan Chen, Na An, Linhe Liu, Yixiu Zhao, Hongxia Zhao, Na Ning, Yan Zhang, Baofeng Yang, Huatuo Zaizao Pills improve myocardial ischemia by inhibiting extracellular calcium influx, Chinese Journal of Natural Medicines, 2026, 24(6), 745−756. doi: 10.1016/S1875−5364(26)61096−5.

View online: https://doi.org/10.1016/S1875−5364(26)61096−5

Chinese Journal of Natural Medicines 24 (2026) 745-756

Contents lists available at ScienceDirect

Chinese Journal of Natural Medicines

journal homepage: www.cjnmcpu.com/

Original article

# Huatuo Zaizao Pills improve myocardial ischemia by inhibiting extracellular calcium influx

Nannan Wang[a,e,Δ], Shifeng Cao[a,Δ], Yu Zhao[b], Yanrong Li[a], Jiewen Zhou[c], Shuyu Liu[a], Huan Chen[a], Na An[a], Linhe Liu[a], Yixiu Zhao[a], Hongxia Zhao[a], Na Ning[d], Yan Zhang[a,*], Baofeng Yang[a,b,*]

[a] *State Key Laboratory of Frigid Zone Cardiovascular Diseases (SKLFZCD), Department of Pharmacology (State Key Labratoray -Province Key Laboratories of Biomedicine-Pharmaceutics of China, Key Laboratory of Cardiovascular Research, Ministry of Education), College of Pharmacy, Harbin Medical University, Harbin 150081, China*

[b] *Research Unit of Noninfectious Chronic Diseases in Frigid Zone (2019RU070), Chinese Academy of Medical Sciences, Harbin 150081, China*

[c] *The First Affiliated Hospital, Guangzhou University of Chinese Medicine, Guangzhou 510530, China*

[d] *Guangzhou Baiyunshan Qixing Pharmaceutical Company Limited, Guangzhou 510530, China*

[e] *Guangzhou Baiyunshan Zhongyi Pharmaceutical Company Limited, Guangzhou 510530, China*

ARTICLE INFO

*Article history:*
Received 12 September 2025
Revised 2 December 2025
Accepted 24 January 2026
Available online 20 June 2026

*Keywords:*
Coronary heart disease
Huatuo Zaizao Pills
Vascular smooth muscle
Calcium channel
Ryanodine receptor
Vasodilation

ABSTRACT

Coronary heart disease (CHD), characterized by impaired coronary artery function, often results in myocardial ischemia, hypoxia, and necrosis, with clinical manifestations such as angina pectoris. Vascular smooth muscle cell (VSMC) hypercontraction, primarily regulated by intracellular calcium ($Ca^{2+}$), plays a central role in pathological coronary vasoconstriction. This study aimed to evaluate the therapeutic effects of Huatuo Zaizao Pills (HTZZ) in alleviating myocardial ischemia caused by abnormal coronary artery contraction and to elucidate the underlying molecular mechanisms. A double-blind, multicenter, randomized, placebo-controlled clinical trial was conducted to assess the efficacy of HTZZ in patients with angina pectoris. *In vivo*, pituitrin-induced acute myocardial ischemia mice and spontaneously hypertensive rats (SHRs) were used to evaluate myocardial and vascular responses to HTZZ. *In vitro*, vasorelaxation mechanisms were investigated using isolated rat mesenteric arterial rings, patch clamp, calcium imaging, and [$^3$H]-ryanodine binding assays. HTZZ significantly reduced the frequency and duration of angina attacks in clinical settings. It improved myocardial ischemia in mice and enhanced vascular elasticity and diastolic function in SHRs. Mechanistically, HTZZ induced vasodilation by inhibiting extracellular $Ca^{2+}$ influx and reducing intracellular $Ca^{2+}$ levels *via* suppression of L-type calcium channels (LTCCs) and ryanodine receptors (RyRs). Long-term HTZZ administration also downregulated LTCC expression at both the protein and mRNA levels. HTZZ effectively alleviates angina and myocardial ischemia by suppressing $Ca^{2+}$-mediated vasoconstriction through targeting LTCCs and RyRs. These findings highlight HTZZ as a promising therapeutic candidate for CHD characterized by coronary vasospasm and ischemia.

## 1. Introduction

Coronary heart disease (CHD), also known as ischemic heart disease (IHD), is primarily caused by impaired coronary artery function [1, 2]. This dysfunction often leads to myocardial ischemia, hypoxia, angina, and, in severe cases, myocardial necrosis as a result of arterial lumen narrowing or obstruction [3, 4]. Despite significant advances in the prevention and treatment of IHD, it remains a major public health burden worldwide owing to its high morbidity and mortality [5].

Atherosclerotic plaque formation and vascular calcification are well-established contributors to the narrowing or occlusion of coronary arteries and are key pathological features of stable coronary artery disease [6, 7]. In addition, acute coronary syndromes, often triggered by elevated coronary artery tension, play a critical role in the onset of angina [8]. The coronary vasculature dynamically regulates myocardial blood flow through vasoconstriction and vasodilation [9]. Excessive or abnormal vasoconstriction—often triggered by factors such as emotional stress, smoking, or alcohol consumption—can exacerbate arterial obstruction, further impair myocardial perfusion, and precipitate angina attacks [10, 11].

Vascular smooth muscle cell (VSMC) is a central mechanism underlying abnormal coronary tension, with intracellular calcium ($Ca^{2+}$) playing a pivotal regulatory role [12, 13]. Inositol 1,4,5-trisphosphate ($IP_3$) and diacylglycerol (DAG) are key second messengers that mediate signal transduction within VSMCs [14]. $IP_3$ activates receptors on the sarcoplasmic reticulum (SR), including $IP_3$ receptors ($IP_3$Rs) and ryanodine receptors (RyRs), promoting $Ca^{2+}$ release from the SR [15]. Additionally, voltage-gated calcium channels (VGCCs) and receptor-operated calcium channels (ROCCs) on the plasma membrane regulate extracellular $Ca^{2+}$ influx [16, 17]. Even minor influxes of extracellular $Ca^{2+}$ can further

* Corresponding author.
*E-mail addresses:* zhangyan@ems.hrbmu.edu.cn (Y. Zhang); yangbf@ems.hrbmu.edu.cn (B. Yang)
Δ These authors contributed equally to this work.

https://doi.org/10.1016/S1875-5364(26)61096-5

stimulate SR $Ca^{2+}$ release, amplifying intracellular $Ca^{2+}$ concentrations [18]. Elevated intracellular $Ca^{2+}$ levels trigger myosin light chain (MLC) phosphorylation, initiating actin–myosin cross-bridge formation and VSMC contraction [19]. Concurrently, DAG activates specific isoforms of protein kinase C (PKC), enhancing the $Ca^{2+}$ sensitivity of contractile filaments and further promoting VSMC contraction [20]. Therefore, modulation of intracellular $Ca^{2+}$ dynamics in VSMCs represents a promising therapeutic strategy for alleviating abnormal coronary vasoconstriction and preventing angina episodes in CHD.

Traditional Chinese medicine and natural small molecules have potential therapeutic value in the treatment of various diseases. Studies have demonstrated that monomeric compounds derived from traditional Chinese medicine exhibit significant therapeutic effects in inflammation [21,22], oxidative stress [23,24], and neuroprotection [25]. Huatuo Zaizao Pills (HTZZ), a classic traditional Chinese medicine formula, are commonly used clinically as an adjuvant treatment during the recovery phase and sequelae of stroke. Research has indicated that HTZZ can also exert significant effects on inflammation, oxidative stress, and neuroprotection [26,27]. However, its impact on vascular function and cardiovascular protection remains unclear. Therefore, this study aimed to systematically evaluate the effects of HTZZ on vascular function and explore its potential mechanisms of action, providing a scientific basis for its application in cardiovascular diseases.

In this study, patients with stable angina were recruited to demonstrate the efficacy of HTZZ in acute myocardial ischemia using a randomized, double-blind, placebo-controlled clinical trial design. Electrocardiographic and myocardial injury parameters were assessed in a pituitrin-induced acute myocardial ischemia model. Hypertension and vascular function were evaluated in spontaneously hypertensive rats. Rat mesenteric arteries were used to evaluate the ion channel mechanisms of HTZZ-induced vasorelaxation.

## 2. Materials and methods

### 2.1. Clinical study design

This double-blind, multicenter, placebo-controlled, randomized clinical trial was conducted at three medical centers in mainland China. The study protocol was approved by the ethics committees of all sites. The trial was registered on the Chinese Clinical Trial Registry (No. ChiCTR2300070770). All participants provided written informed consent. The trial flow diagram is presented in Fig. S2.

### 2.2. Participants and sample size calculation

Detailed inclusion and exclusion criteria are provided in Supporting Information. According to preliminary clinical results, we assumed that the effective rate was 85% in the HTZZ group and 55% in the placebo group. A total of 40 participants per arm could achieve a power level above 0.80 at a significance level of 0.05. We inflated the sample size to 96 considering a dropout rate of 20%.

### 2.3. Intervention and outcomes

Patients were randomly assigned in a 1 ∶ 1 ratio to receive either HTZZ or a matching placebo (8 g once, 3 times per day). The duration of the treatment course was 4 weeks for all participants. Detailed information on randomization and masking is provided in Supporting Information. The primary outcome was to validate the clinical efficacy of HTZZ in the treatment of angina pectoris, including the change in frequency and duration of angina before and after treatment.

### 2.4. Materials

Arterial smooth muscle cells (A10) were purchased from the American Type Culture Collection (ATCC). CAY10441, ODQ, and tetraethylammonium (TEA) chloride were purchased from Selleck (Shanghai, China). Phenylephrine (PE), CsCl, $CaCl_2$, $MgCl_2 \cdot 6H_2O$, HEPES, CsOH, Mg-ATP, and EGTA were purchased from Sigma-Aldrich Co., Ltd. (St. Louis, USA). Acetylcholine (ACh) was purchased from Meilun Biotech (Dalian, China). BAPTA-AM, 2-aminoethyl diphenylborinate (2-APB), thapsigargin, NNC 55-0396, ruthenium red, 4-aminopyridine (4-AP), glibenclamide, verapamil, and N($\omega$)-nitro-L-arginine methyl ester (L-NAME) were purchased from MedChemExpress, Shanghai, China. $BaCl_2$ was purchased from HengXing Chemical Reagent, Tianjin, China. he Fluo-4 Calcium Assay Kit and bicinchoninic acid protein assay reagent kit (BCA kit) were purchased from Beyotime Biotechnology (Shanghai, China). SYBR Green Real-time PCR Master Mix and ReverTra AceTM qPCR RT Kit were purchased from TOYOBO (Shanghai) Biotech Co., Ltd. (Shanghai, China). TBS buffer powder was purchased from Boster Biological Technology (Wuhan, China).

### 2.5. Animals and treatment

Adult male Sprague-Dawley (SD) rats (6–8 weeks old, body weight 200–250 g) and male KM mice (8 weeks old) were purchased from Liaoning Changsheng Biotechnology for experimental studies (license number: SCXK(Liao)2020-0001).

Spontaneously hypertensive rats (SHRs; 8 weeks old) and Wistar Kyoto rats (WKYs; 8 weeks old) were obtained from Beijing Vital River Laboratory Animal Technology (license number: SCXK(Jing)2021-0006). All animals were housed under controlled conditions at a constant temperature of 25 ± 3 °C with a humidity range of 50%–70% under a 12-h light/dark cycle. The experiments were conducted in compliance with the Regulations on the Management of Experimental Animals in Heilongjiang Province (dated December 16, 2016) and were approved by the Ethics Committee for Animal Experimentation of Harbin Medical University.

KM mice were randomly divided into six groups: control (0.9% saline), model (0.9% saline), isosorbide mononitrate (ISMN, 5.2 $mg \cdot kg^{-1} \cdot d^{-1}$), HTZZ low dose (1.55 $mg \cdot kg^{-1} \cdot d^{-1}$), HTZZ middle dose (3.1 $g \cdot kg^{-1} \cdot d^{-1}$), and HTZZ high dose (6.2 $g \cdot kg^{-1} \cdot d^{-1}$). Mice were administered HTZZ by gavage daily for 1 week. After the final administration, mice were anesthetized with Alfaxan (125–400 $mg \cdot kg^{-1}$). They then received pituitrin by intraperitoneal injection (0.9 U/10 g, except for the control group) to record electrocardiographic signals immediately. After 30 min, blood samples were collected and centrifuged for serum enzyme assays. Hearts were excised and rinsed in ice-cold isotonic saline. Blood and heart samples were stored at −80 °C prior to further analysis.

SHRs and WKYs were randomly divided into four groups: SHR (0.9% saline), SHR + HTZZ (HTZZ 4 $g \cdot kg^{-1} \cdot d^{-1}$), WKY (0.9% saline), and WKY + HTZZ (HTZZ 4 $g \cdot kg^{-1} \cdot d^{-1}$). Rats were administered HTZZ by gavage daily for 2 weeks. After the final administration, their blood pressure was measured using a tail blood pressure meter (BP2010, Softron, Beijing, China).

### 2.6. Measurement of vascular tension

SD rats were anesthetized with sodium pentobarbital (40 $mg \cdot kg^{-1}$, i.p.). After anesthesia, the animals were euthanized by cervical dislocation, and the intact mesenteric artery was quickly isolated and transferred to cold PSS (4 °C) preoxygenated with 95% $O_2$ and 5% $CO_2$. The adipose tissue and residual blood on the

mesenteric artery were promptly removed, and a 2-mm-long section of the vessel ring was excised. To construct an endothelium-denuded vascular ring model, a mechanical method was employed. Specifically, rat whiskers with a minimum diameter of 80 μm were slowly rubbed against the inner surface of the vascular ring to remove the endothelial cells. The absence of vasorelaxation in response to 1 μmol·$L^{-1}$ ACh indicated successful endothelial cell disruption. The mesenteric artery ring was fixed with two metal wires threaded through it in a bath containing precooled PSS continuously supplied with 95% $O_2$ and 5% $CO_2$ using a microvascular tension measurement device (Myograph System DMT 620M). The mesenteric artery rings were allowed to equilibrate for vascular standardization before undergoing a wake-up procedure involving reactivation of the mechanical, functional, and signaling functions of the vessel with PE and high-$K^+$ salt solution (KPSS). The isometric systolic tension of the mesenteric artery was recorded using the DMT620M microvascular tension measurement device.

### 2.7. Recording of electrocardiogram

Heart rate and S-T segment height were measured using a BL420F Biopotential Acquisition System. The electrocardiogram was recorded for 10 min.

### 2.8. Flow cytometric analysis

A10 cells in the logarithmic growth phase were digested and centrifuged at 1000 r·$min^{-1}$ for 3 min. Cells were washed three times with $Ca^{2+}$-free Tyrode's solution and resuspended in same solution. Fluo-4 AM $Ca^{2+}$ fluorescent probe (Beyotime, S1061M) was dissolved in $Ca^{2+}$-free Tyrode's solution (1 : 500) and added to the A10 cells. Cells were incubated at 37 °C for 30 min and then centrifuged at 1000 r·$min^{-1}$ for 3 min. The supernatant was removed, and cells were resuspended in $Ca^{2+}$-free Tyrode's solution. Cells were mixed and aliquoted into light-protected centrifuge tubes, each containing 200 μL. Cells were divided into four groups: control, model, HTZZ, and verapamil. The HTZZ group was treated with 2.0 mg·$mL^{-1}$ HTZZ, and the verapamil group was treated with 1 μmol·$L^{-1}$ verapamil, each for 20 min. The control and model groups were treated with an equal volume of $Ca^{2+}$-free Tyrode's solution for 20 min.

A flow cytometer was used to measure the baseline fluorescence intensity of cells. The analysis speed was adjusted appropriately to ensure that a suitable number of cells were analyzed. The baseline fluorescence intensity of each group was recorded for 5 min. For the model, HTZZ, and verapamil groups, KCl (60 mmol·$L^{-1}$) and $CaCl_2$ (1.8 mmol·$L^{-1}$) were added to the light-protected centrifuge tubes to trigger $Ca^{2+}$ influx in the cells (an equal volume of $Ca^{2+}$-free Tyrode's solution was added to the control group), and fluorescence intensity was immediately measured. Fluorescence intensity were recorded for five minutes.

### 2.9. Whole-cell patch clamp experiments

All whole-cell patch-clamp experiments were performed using an Axopatch 700B amplifier. Whole-cell currents were sampled at 1 kHz and filtered at 2 kHz. The ICa,L in A10 cells was recorded in extracellular solution containing (in mmol·$L^{-1}$): 120 TEA, 10 HEPES, 1 $MgCl_2 \cdot 6H_2O$, 10 CsCl, 10 glucose, and 1.8 $CaCl_2$ (pH adjusted to 7.30 with CsOH). The pipette solution contained (in mmol·$L^{-1}$) 120 CsCl, 1 $MgCl_2 \cdot 6H_2O$, 40 CsOH, 5 Mg-ATP, 11 EGTA, and 10 HEPES (pH adjusted to 7.30 with CsOH). The cell was maintained at a membrane potential of −40 mV, and a gradually increasing depolarizing voltage from −30 mV to 60 mV was applied to record the L-type calcium channel currents of A10 cells.

### 2.10. Western blot

Total protein was extracted from tissues or cells using RIPA lysis buffer (P0013B, Beyotime, Beijing, China). Protein concentration was quantified using a BCA Protein Concentration Measurement Kit (P0011, Beyotime, Beijing, China) to standardize the loading mass. SDS-PAGE Protein Loading Buffer (5 ×) (P0015, Beyotime, Beijing, China) was added, and the samples were heated at 100 °C for 7 min. Electrophoresis was performed on SDS-polyacrylamide gels. Proteins were then transferred to nitrocellulose membranes and blocked in 5% skim milk. The primary antibodies used in this study included anti-CACNA1C (DF2267, Affinity, Jiangsu, China, 1 ∶ 1000), anti-Phospho-CACNA1C (AF8363, Affinity, Jiangsu, China, 1 ∶ 1000), anti-GAPDH (10494-1-AP, Proteintech, Wuhan, China, 1 ∶ 10 000). Membranes were incubated with primary antibodies overnight at 4 °C. Membranes were subsequently incubated with fluorescence-conjugated anti-rabbit IgG or anti-mouse IgG secondary antibodies (1 ∶ 10 000, LI-COR Bio-Science, Lincoln, USA) at room temperature away from light for 1 h. Protein bands were analyzed using the Odyssey infrared imaging system (LI-COR, USA).

### 2.11. qRT-PCR

Total RNA was isolated from rat thoracic aorta and A10 cells using TRIzol reagent (15596018CN, Invitrogen, CA, USA). The concentration and purity of the extracted RNA were determined using a NanoDrop 8000 (Thermo Fisher, Waltham, MA, USA), and RNA was reverse-transcribed to cDNA using a reverse transcription kit (FSQ-101, Toyobo, Osaka, Japan). Real-time PCR was performed using Toyobo Universal SYBR qPCR Master Mix (QPX-201, Toyobo, Osaka, Japan). All cDNA samples were prepared in a 20-μL reaction system. Reaction conditions were as follows: initial denaturation at 95 °C for 5 min; 40 cycles of 95 °C for 30 s, 65 °C for 30 s, and 72 °C for 30 s. The comparative cycle threshold (Ct) method was used to analyze target gene expression using the $2^{-\Delta\Delta CT}$ method.

### 2.12. RNA-sequencing analysis

Rat mesenteric artery was collected for RNA sequencing. Briefly, total RNA from each sample was extracted using TRIzol reagent. A total of 1 μg of RNA per sample was used as input material for RNA sample preparation. Sequencing libraries were generated using the NEBNext® Ultra™ RNA Library Prep Kit for Illumina® (NEB, USA). Index codes were added to the sequence attributes for each sample. Finally, PCR products were purified (AMPure XP system). Library quality was assessed using an Agilent Bioanalyzer 2100 system and quantified with a 2.0 Fluorometer (Invitrogen, Carlsbad, CA, USA).

### 2.13. Construction and analysis of Protein-Protein Interaction (PPI) network

PPI network analysis was carried out using the STRING database (http://string-db.org/), generating the high-confidence PPI network (combined score ≥ 0.7). Cytoscape 3.9.1 was used for data analysis and visualization. PPI sub-networks were analyzed using the MCODE (Molecular Complex Detection) plugin in Cytoscape 3.9.1. MCODE parameters were set as follows: degree cutoff = 2, node score cutoff = 0.2, k-core = 2, and max depth = 100.

### 2.14. Pathway enrichment analysis and visualization

The Database for Annotation, Visualization and Integrated Discovery (DAVID) was applied in Gene Ontology (GO) annotation and KEGG pathway analysis. The false discovery rate (FDR) was used to show the enrichment significance.

*2.15. Doppler ultrasound*

The ascending aorta, located 3 cm above the aortic valve, was imaged using the parasternal long-axis view. The systolic aortic diameter (As) was measured at the end of the T wave on the ECG. The diastolic aortic diameter (Ad) was measured at the end of the P wave on the ECG using M-mode echocardiography. These measurements were performed using a Doppler ultrasound imaging system (VINNO, Suzhou, China). Average values were derived from three measurements of each diameter for data analysis. Three elastic indices of aortic stiffness, namely aortic distensibility (D), stiffness index (β), and elastic modulus (Ep), were calculated respectively as D = 2(As-Ad)/[Ad (Ps-Pd)], β = ln(Ps/Pd)/[(As-Ad)/Ad], and Ep = (Ps-Pd)/[(As-Ad)/Ad], where Ps = systolic blood pressure, Pd = diastolic blood pressure, and ln = natural logarithm.

*2.16. Determination of blood pressure*

Blood pressure changes in experimental animals were measured using an intelligent non-invasive blood pressure monitor. The animals were placed in a quiet, temperature-controlled environment. After securing the animals and allowing them to acclimate to the measurement conditions, their tails were exposed. The pressure sensor of the non-invasive blood pressure monitor was then placed around the tail base of each animal. Sequential inflation and deflation were performed. After 14 days of gavage, systolic and diastolic pressures of the tail arteries in each group of experimental animals were measured. To ensure data accuracy and repeatability, measurements were taken three times consecutively, and the average value was recorded.

*2.17. Enzyme-linked immunosorbent assays (ELISA)*

Serum was obtained from whole blood by centrifugation at 1200 × g at 4 °C for 20 min. Serum levels of creatine kinase-MB (CK-MB) (Cat No. EM0929) and malondialdehyde (MDA) (Cat No. EM1723-1) in mouse serum were measured using the corresponding mouse ELISA kits (Wuhan Fine Biotech Co., Ltd., Wuhan, China). Serum levels of angiotensin I-converting enzyme (ACE) (Cat No. EM0011) and angiotensin II (Ang II) (Cat No. EM2050) in rat serum were measured using the corresponding rat ELISA kits (Wuhan Fine Biotech Co., Ltd., Wuhan, China).

*2.18. Determination of lactate dehydrogenase (LDH) in the serum*

Serum LDH levels (Cat No. A020-2-2) in mouse serum were measured using an LDH assay kit (Nanjing Jiancheng Bioengineering Institute, Shanghai, China).

*2.19. Measurement of the cytosolic [$Ca^{2+}$] in VSMCs*

A10 cells were cultured and washed three times with $Ca^{2+}$-free Tyrode's solution. Then, Fluo-4 AM $Ca^{2+}$ fluorescent probe (Beyotime, S1061M) was dissolved in $Ca^{2+}$-free Tyrode's solution (1 ∶ 500) and added to the A10 cells. The cells were incubated at 37 °C in darkness for 30 min. The $Ca^{2+}$-free Tyrode's solution was discarded The cells were washed three times with warm $Ca^{2+}$-free Tyrode's solution (37 °C). Subsequently, 1 mL of warm $Ca^{2+}$-free Tyrode's solution (37 °C) was added. The fluorescence intensity of fluo-4 AM in the cells was measured.

*2.20. [$^3$H]ryanodine binding*

A10 cells were divided into three groups: HTZZ group, ruthenium red (RR) group, and control group. The HTZZ group was treated with HTZZ (2 mg·mL$^{-1}$) and incubated for 20 min. The RR group was treated with ruthenium red (10 μmol·L$^{-1}$) and incubated for 20 min. The control group was treated with an equal volume of PBS and incubated for 20 min. The endoplasmic reticulum was extracted using an Endoplasmic Reticulum Extraction Kit (MERCK ER0100) according to the manufacturer's instructions. Endoplasmic reticulum sample solution (1 μg·μL$^{-1}$) was mixed with 10 nmol·L$^{-1}$ [$^3$H]ryanodine and ryanodine in 200 μL of binding buffer. The mixture was incubated at 37 °C with gentle shaking for 3 h in a constant-temperature water bath and then cooled on ice to terminate the binding reaction. The filtration device was washed, and a glass fiber filter was placed inside. The sample was filtered, and the filter membrane was washed three times with cold washing buffer. Radioactivity was measured using liquid scintillation counting.

*2.21. Statistical analysis*

All data were statistically analyzed using SPSS 25.0 software. The primary analysis was conducted in the Full Analysis Set (FAS). The Per-Protocol Set (PPS) was also analyzed as a sensitivity analysis. In clinical data analysis, categorical data were evaluated using the chi-square test or Fisher's exact test as appropriate. Continuous data are presented as mean ± SD. The number of angina attacks and duration of angina attacks were repeated-measurement outcomes; these outcomes were therefore assessed using analysis of covariance (ANCOVA), with group as a fixed effect and the baseline value as a covariate. Given the potential between-group difference in sex distribution ($P$ = 0.178), sensitivity analysis was also conducted using ANCOVA, with group as a fixed effect and the baseline value, sex, and the interaction term between sex and group as covariates. If the interaction term was not significant ($P \geq 0.05$), it was excluded, and the model was refitted to report sex-adjusted mean differences with 95% confidence intervals (CIs). Data analysis used a last observation carried forward (LOCF) approach with missing data at any time point imputed from the most recently available value.

*In vivo* results are presented as mean ± SEM. For continuous variables following a normal distribution, one-way ANOVA was used to compare means among multiple samples, and *post hoc* pairwise comparisons were conducted using the LSD method. For variables not complying with a normal distribution, the Kruskal-Wallis H test was used to compare differences among groups, and the Nemenyi test was applied in *post hoc* pairwise comparisons. $P < 0.05$ was considered statistically significant.

Differentially expressed genes (DEGs) in mouse mRNA sequencing data were analyzed using R software (v4.4.1) with the DESeq2 package. Gene Set Enrichment Analysis (GSEA) was performed using GSEABase.

## 3. Results

*3.1. The plasma chemical profiles of Huatuo Zaizao Pills*

Plasma chemical profiles of Huatuo Zaizao Pills were analysed by LC-MS/MS. The chemical constituents were identified by comparing to standards. The identified chemicals included quinic acid (1), loganic acid (3), 5-caffeylquinic acid (4), 1,3-dicaffeoylquinic acid (8), kaempferol 3-O-sophoroside (12), ferulic acid (16), rutin (17), quercetin-7-O-β-*D*-glucopyranoside (19), kaempferol-3-O-β-*D*-glucopyranoside (23), kaempferol-7-O-β-*D*-glucopyranoside (24), isorhamnetin-3-rutinoside (26), isorhamnetin (32).

The detailed preparation method of HTZZ plasma and MS information of these components could be found in Supplementary Materials.

*3.2. Efficacy of HTZZ in reducing angina frequency and duration: a randomized clinical trial*

To demonstrate the efficacy of HTZZ in acute myocardial

ischemia, a randomized, double-blind, placebo-controlled clinical trial involving 96 patients with stable angina was conducted. The two arms were comparable in baseline characteristics (all $P > 0.05$, Table 1).

**Table 1** Characteristics of participants.

| Characteristics | | HTZZ group ($n$ = 48) | Placebo group ($n$ = 48) | $P$ |
|---|---|---|---|---|
| Sex, no.% | | | | |
| | Male | 11 (22.9) | 17 (35.4) | |
| | Female | 37 (77.1) | 31 (64.6) | 0.178 |
| Age, years, means ± SD | | 55.35 ± 6.85 | 55.33 ± 6.40 | 0.241 |
| Weight, means ± SD | | 67.55 ± 8.08 | 68.27 ± 11.60 | 0.920 |
| Height (cm), means ± SD | | 162.77 ± 6.52 | 165.04 ± 8.20 | 0.137 |
| Duration of disease (Month), means ± SD | | 48.46 ± 50.90 | 46.13 ± 41.61 | 0.806 |
| Class I and Class II exertional angina, no.% | Ⅰ | 24 (50.0) | 28 (58.3) | 0.415 |
| | Ⅱ | 24 (50.0) | 20 (41.7) | |
| Heart rate (beats per minute), means ± SD | | 69.77 ± 9.88 | 72.52 ± 9.00 | 0.157 |
| Number of angina attacks (times/week) | | 6.10 ± 2.75 | 5.58 ± 2.11 | 0.300 |
| Duration of angina attacks (minutes/episode) | | 5.73 ± 1.94 | 5.48 ± 1.60 | 0.493 |

HTZZ: Huatuo Zaizao Pills; SD: standard deviation; $P < 0.05$ was considered as statistically significant.

In the FAS, both the HTZZ group and the placebo group showed reductions in the frequency and duration of angina attacks. In the HTZZ group, the frequency of angina attacks decreased from 6.10 ± 2.75 (times/week) at baseline to 2.31 ± 1.79 (times/week) after 4 weeks of treatment. Similarly, the duration of angina episodes decreased from 5.73 ± 1.94 (min/episode) to 2.58 ± 1.80 (min/episode). In the placebo group, the frequency of angina attacks decreased from 5.58 ± 2.11 (times/week) to 3.52 ± 1.54 (times/week), and the duration of episodes decreased from 5.48 ± 1.60 (min/episode) to 3.90 ± 1.64 (min/episode).

Compared with the placebo group, HTZZ intervention for 4 weeks significantly reduced both the frequency of angina attacks and the duration of episodes, with effect sizes of −1.38 (−1.98, −0.77) and −1.41 (−2.05, −0.76), respectively. A similar trend was observed in the PPS analysis (both $P < 0.001$, Table 2).

### *3.3. HTZZ ameliorates abnormal electrocardiogram and myocardial injury in a dose-dependent manner in mice with acute myocardial ischemia induced by Pituitrin*

To investigate the effect of HTZZ on acute myocardial ischemia, this study used a pituitrin-induced acute myocardial ischemia model. The protective role of HTZZ against acute myocardial ischemia was evaluated by examining its impact on the electrocardiogram of mice during acute myocardial ischemia and on serum myocardial injury biomarkers, including LDH, CK-MB, and MDA, at 24 h post-ischemia. Mice were treated with different doses of HTZZ (1.55, 3.1, or 6.2 $g \cdot kg^{-1} \cdot d^{-1}$), ISMN (5.2 $mg \cdot kg^{-1} \cdot d^{-1}$), or saline for seven consecutive days. After the treatment period, they were intraperitoneally injected with pituitrin (90 $U \cdot kg^{-1}$ ) or an equivalent volume of saline to induce acute myocardial ischemia (Fig. 1A).

After injection of pituitrin, the T-wave height in the mouse electrocardiogram increased and the heart rate slowed; however, after seven days of administration, both HTZZ (1.55, 3.1, 6.2 $g \cdot kg^{-1} \cdot d^{-1}$) and ISMN (5.2 $mg \cdot kg^{-1}$) reduced the T-wave height (Figs. 1B) and improved the heart rate (Fig. 1D), with HTZZ demonstrating a dose-dependent effect. Furthermore, after seven days of administration, HTZZ (1.55, 3.1, and 6.2 $g \cdot kg^{-1}$) and ISMN (5.2 $mg \cdot kg^{-1}$) significantly reduced serum levels of Lactate Dehydrogenase (LDH), Creatine Kinase-Muscle/Brain (CK-MB), and Malondialdehyde (MDA) in mice with acute myocardial ischemia compared to the model group (Figs. 1E, 1F, 1G), with HTZZ demonstrating a dose-dependent effect. These data suggest that HTZZ may improve acute myocardial ischemia through coronary artery vasodilation.

**Table 2** Treatment outcomes in study population.

| Outcomes | HTZZ group | Placebo group | Adjusted mean difference (95% CI)[a] | $P$ [a] |
|---|---|---|---|---|
| **FAS** | $n$ = 48 | $n$ = 48 | | |
| Number of angina attacks (times/week) | 2.31 ± 1.79 | 3.52 ± 1.54 | −1.38 (−1.98, −0.77) | < 0.001 |
| Duration of angina attacks (minutes/episode) | 2.58 ± 1.80 | 3.90 ± 1.64 | −1.41 (−2.05, −0.76) | < 0.001 |
| **PPS** [b] | $n$ = 43 | $n$ = 44 | | |
| Number of angina attacks (times/week) | 2.09 ± 1.62 | 3.48 ± 1.55 | −1.40 (−2.02, −0.77) | < 0.001 |
| Duration of angina attacks (minutes/episode) | 2.30 ± 1.64 | 3.80 ± 1.65 | −1.52 (−2.18, −0.86) | < 0.001 |

HTZZ: Huatuo Zaizao Pills; SD: standard deviation; FAS, full analysis set; PPS, per-protocol set. [a] Data are presented as unadjusted mean ± SD. Between-group differences were analyzed using analysis of covariance (ANCOVA), with treatment group as a fixed effect and baseline values as covariates. The model was fitted to report baseline adjusted mean differences with 95% confidence intervals (CIs). $P < 0.05$ was considered as statistically significant. [b] In the HTZZ group, 2 were lost to follow-up and 3 were unwilling to continue treatment. In the placebo group, 1 was lost to follow-up and 3 had adverse events. These participants were excluded from PPS.

### 3.4. HTZZ Improves hypertension and vascular relaxation function in spontaneously hypertensive rats

SHRs exhibit impaired vascular relaxation and abnormally elevated vascular tension. Therefore, to determine whether HTZZ can improve vascular relaxation and inhibit abnormal vasoconstriction, we used SHRs to evaluate the effects of HTZZ on blood pressure, aortic elasticity, and vascular relaxation function, thereby comprehensively assessing its impact on vasorelaxation. Following 14 days of HTZZ administration (4 g·kg$^{-1}$·d$^{-1}$), significant reductions in both systolic and diastolic blood pressure were observed compared with SHRs (Figs. 2A, 2B).

Sustained hypertension induces progressive deterioration of aortic compliance, characterized by diminished vasodilatory capacity and impaired arterial elastic recoil function. To quantitatively evaluate vascular stiffness in our experimental model, we performed high-resolution Doppler ultrasonography to measure dynamic changes in aortic diameter during the cardiac cycle. Following 14 days of HTZZ administration (4 g·kg$^{-1}$·d$^{-1}$), HTZZ significantly increased the difference in aortic outflow tract diameters between diastole and systole in SHRs (Figs. 2C, 2D). Based on the aforementioned differences in aortic diameters during diastole and systole, along with blood pressure data, three indices for aortic stiffness evaluation were derived: Elastic modulus (Ep), Stiffness index (β), and Distensibility (D) (Table S4). As shown in Figs. 2E–2G, after 14 days of administration, HTZZ (4 g·kg$^{-1}$·d$^{-1}$) reduced the stiffness index of SHR aortas and increased aortic vascular elasticity. After 14 days of HTZZ treatment (4 g·kg$^{-1}$·d$^{-1}$), vascular tension assays demonstrated significantly potentiated vasodilatory responses to both sodium nitroprusside (SNP) (Figs. 2H, 2I) and acetylcholine (ACh) (Figs. S3A, 3B), indicating enhanced endothelium-dependent and -independent vascular relaxation. The above results suggest that HTZZ ameliorate hypertension in SHR rats by improving vascular diastolic function.

### 3.5. Transcriptomic sequencing analysis of the therapeutic targets of HTZZ in SHRs

To explore the mechanism by which HTZZ improves vascular diastolic function, we conducted mRNA sequencing to identify differentially expressed mRNAs in SHRs following treatment with HTZZ. Gene Ontology (GO) annotation and enrichment analysis were performed on the 236 DEGs (HTZZ group *vs* SHR group) (Figs. S4A, S4B). The top ten results were selected based on the -$\log_{10}$ FDR (all $P < 0.01$). GO annotation for these target DEGs indicated associations with various biological processes, including chromosome segregation, calcium ion transmembrane transport, calcium ion import across the plasma membrane, calcium ion transport, and calcium ion import (Fig. 3A). These biological processes are mainly executed through molecular functions, including microtubule binding, protease binding, voltage-gated calcium channel activity involved in regulation of presynaptic cytosolic calcium levels, phospholipid binding, and enzyme regulator activity (Fig. 3B). The functional impacts of these genes are predominantly exerted in the voltage-gated calcium channel complex, extracellular space, very-low-density lipoprotein particle, chylomicron, and high-density lipoprotein particle (Fig. 3C). As can be seen in the KEGG analysis (Fig. 3D), the DEGs were mainly enriched in cardiac function-related pathways, including vascular smooth muscle contraction, calcium signaling pathway, MAPK signaling pathway, renin secretion, cholesterol metabolism, aldosterone synthesis and secretion, adrenergic signaling in cardiomyocytes, and complement and coagulation cascades. Owing to their important role in cardiac function, two pathways were visualized using GSEA: the calcium signaling pathway and vascular smooth muscle contraction (Figs. 3E, 3F). In the primary PPI network, there exist 146 nodes and 767 edges (Fig. 3G). We further applied MCODE method to extract important sub-networks (Figs. 3H, 3I, 3J), generating the top 3 clusters, namely cluster 1 (21

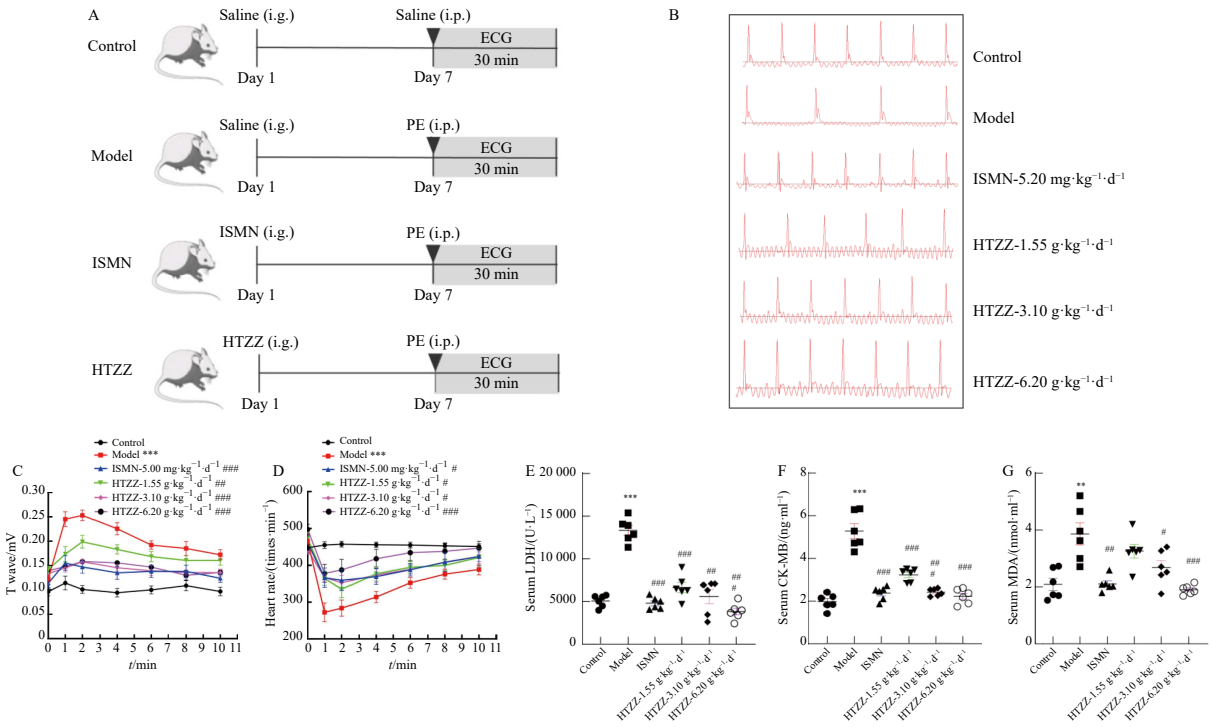


**Fig. 1** HTZZ improves acute myocardial ischemia. (A) Schematic representation of the acute myocardial ischemia mice experiment protocol. (B) Typical electrocardiogram (ECG) traces 10 minutes after intraperitoneal injection of pituitrin. (C) Prophylactic treatment with HTZZ at doses of 1.55, 3.10, and 6.20 g·kg$^{-1}$·d$^{-1}$ for 7 consecutive days or therapeutic treatment with Isosorbide Mononitrate (ISMN) decreased T wave height of mice with acute myocardial ischemia induced by pituitrin ($n$ = 8). (D) Prophylactic treatment with HTZZ at doses of 1.55, 3.10, and 6.20 g·kg$^{-1}$·d$^{-1}$ for 7 consecutive days or therapeutic treatment with ISMN decreased the heart rate in mice with acute myocardial ischemia induced by pituitrin ($n$ = 8). (E) Serum lactate dehydrogenase (LDH) levels ($n$ = 6). (F) Serum creatine kinase-MB (CK-MB) levels ($n$ = 6). (G) Serum CK-MB levels ($n$ = 6). Data are presented as mean ± SEM. $^{***}P < 0.001$ *vs* Control, $^{**}P < 0.01$ *vs* Control, $^{*}P < 0.05$ *vs* Control. $^{\#\#\#}P < 0.001$ *vs* Model, $^{\#\#}P < 0.01$ *vs* Model, $^{\#}P < 0.05$ *vs* Model.

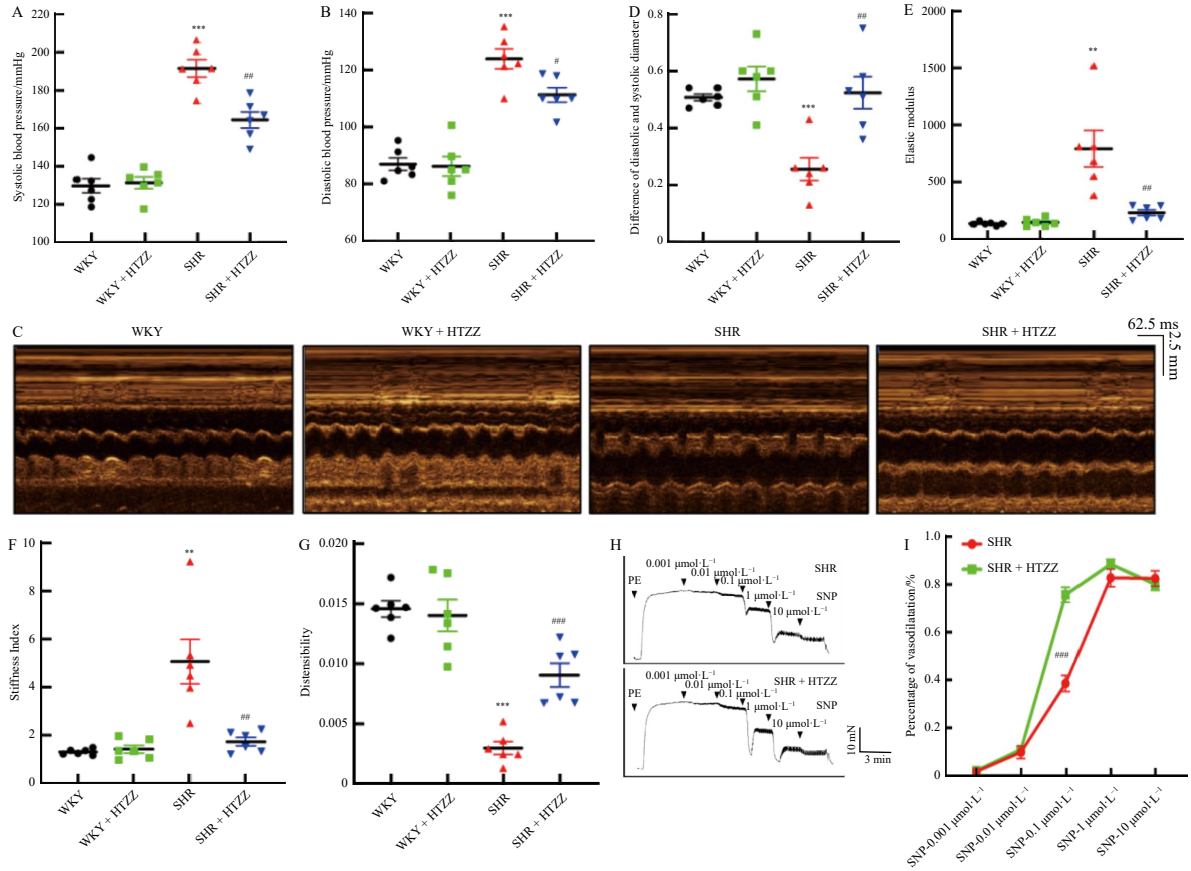


**Fig. 2** HTZZ improves hypertension and vascular diastolic function. (A) Systolic blood pressure of rats in each group. ($n$ = 6). (B) Diastolic blood pressure of rats in each group. ($n$ = 6) (C, D) Representative ultrasound images of aortic outflow tract and summarized data of the difference of diastolic and systolic diameter. ($n$ = 6) (E, F, G) Summarized data of elastic modulus, stiffness index, and distensibility of aortic outflow tract and aortic arch. ($n$ = 6) (H, I) Representative tension recording image of SNP-induced vasodilation with gradient concentrations and corresponding statistical graph. ($n$ = 7) Data are shown as mean ± SEM. $^{*}P < 0.05$ *vs* WKY, $^{**}P < 0.01$ *vs* WKY, $^{***}P < 0.001$ *vs* WKY, $^{\#}P < 0.05$ *vs* SHR, $^{\#\#}P < 0.01$ *vs* SHR, $^{\#\#\#}P < 0.001$ *vs* SHR.

nodes and 194 edges), cluster 2 (21 nodes and 130 edges), and cluster 3 (12 nodes and 65 edges), presented in Table 3. Cluster 1 was mainly enriched in cardiac function-related pathways such as motor proteins. Cluster 2 was mainly enriched in cardiac function-related pathways such as complement and coagulation cascades, cholesterol metabolism, and platelet activation. Cluster 3 was mainly enriched in the MAPK signaling pathway, arrhythmogenic right ventricular cardiomyopathy, and cardiac muscle contraction. These results suggest that HTZZ may improve vascular diastolic function by inhibiting calcium signaling in vascular smooth muscle.

### *3.6. HTZZ induces vasorelaxation in rat mesenteric arteries in a concentration-dependent and endothelium-independent manner*

To further investigate the vasomodulatory effects of Huatuo Zaizao Pills (HTZZ), we assessed their influence on rat mesenteric arterial rings precontracted with either phenylephrine (PE, 5 μmol·L$^{-1}$) or high-potassium physiological saline solution (KPSS, 60 mmol·L$^{-1}$). Endothelial integrity was verified by the vasodilatory response to acetylcholine (Ach, 1 μmol·L$^{-1}$), which induced robust relaxation in endothelium-intact vessels (Fig. 4A).

HTZZ (0.5, 1, 2 mg·mL$^{-1}$) elicited significant, concentration-dependent vasorelaxation in both endothelium-intact (Fig. 4A, 4E) and endothelium-denuded (Fig. 4B, 4F) mesenteric arterial rings following PE-induced preconstriction. This vasodilatory response persisted even in the presence of L-NAME, an endothelial nitric oxide synthase inhibitor (Fig. S5A, S5C), suggesting that the effect of HTZZ is independent of nitric oxide signaling. Similarly, HTZZ also reversed vasoconstriction induced by KPSS in a concentration-dependent manner regardless of endothelial status (Fig. 4C, 4D, 4G, 4H), and was unaffected by L-NAME pretreatment (Fig. S5B, S5D), further supporting an endothelium-independent mechanism.

To directly compare the vasodilatory efficacy of HTZZ across different vascular conditions, we constructed concentration–response curves in endothelium-intact, endothelium-denuded, and L-NAME-pretreated vessels. The curves revealed no significant differences in HTZZ-mediated relaxation among the three groups under either PE- or KPSS-induced contraction conditions (Figs. 4I, 4J), confirming that the vasorelaxant effects of HTZZ do not rely on endothelial-derived factors.

Additionally, in a separate set of experiments, HTZZ (0.5, 1, 2 mg·mL$^{-1}$) dose dependently attenuated PE- and KPSS-induced vasoconstriction in both endothelium-intact and denuded arteries, as well as in the presence of L-NAME (Figs. S6A–6F), and the overall inhibitory effects on contractile tension were comparable across groups (Figs. S6J, S6N). Together, these findings indicate that HTZZ induces potent vasorelaxation through an endothelium-independent pathway, contributing to its potential therapeutic effects in ischemic vascular disorders.

### *3.7. HTZZ induces vasorelaxation through inhibiting RyRs and LTCCs*

Next, we investigated the underlying mechanisms of HTZZ-induced vasodilation. We systematically employed a panel of pharmacological inhibitors targeting key pathways involved in vascular smooth muscle contraction and relaxation, including ODQ (a soluble guanylate cyclase inhibitor), CAY10441 (a prostacyclin receptor antagonist), verapamil (an L-type calcium channel blocker), NNC 55-0396 (a T-type calcium channel blocker), 2-

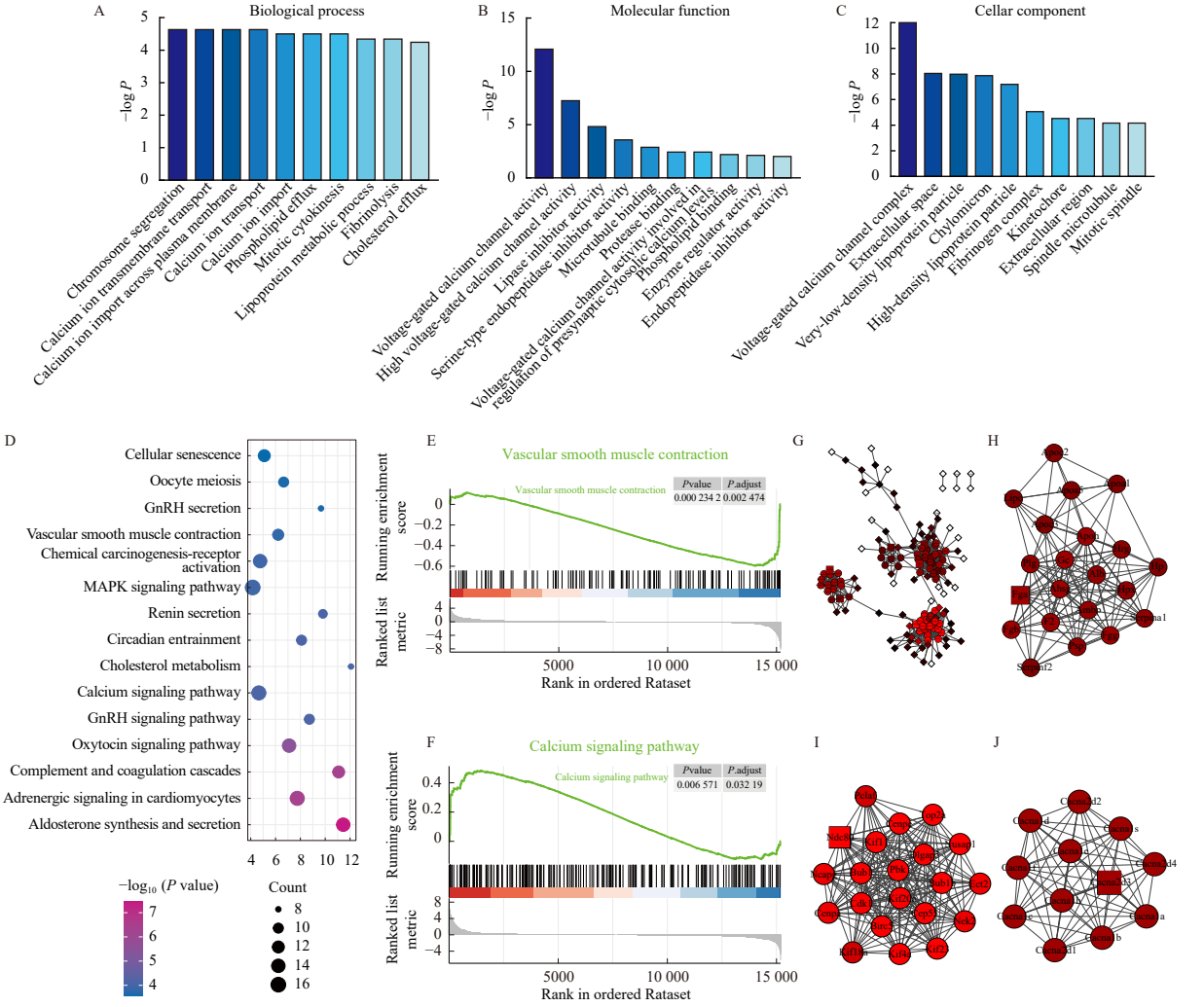


**Fig. 3** Screening of the mRNAs in the mesenteric artery of SHR and HTZZ groups. (A) Representative tension recording image of HTZZ (2 mg·mL$^{-1}$) on vasodilation of endothelium-intact vascular rings preconstricted by Ruthenium Red for 30 min. (B–C) Perform GO enrichment analysis based on the GO database, and conduct enrichment analysis for differential genes among samples in terms of biological process, molecular function, and cellular component. (D) Bubble plot of KEGG enrichment for upregulated and downregulated differentially expressed genes. (E) GSEA analysis for genes highly related to vascular smooth muscle contraction. (F) GSEA analysis for genes highly related to calcium signaling pathways. (G–J) PPI network analysis.

APB (an IP3 receptor inhibitor), ruthenium red (an RyR inhibitor), 4-AP (a voltage-gated potassium channel blocker), TEA (a calcium-activated potassium channel blocker), glibenclamide (an ATP-sensitive potassium channel blocker), $BaCl_2$ (an inward rectifier potassium channel blocker), BAPTA-AM (a calcium chelator), and thapsigargin (a sarco/endoplasmic reticulum $Ca^{2+}$ -ATPase inhibitor). By assessing their modulatory effects on HTZZ-mediated vasodilation, we elucidated the potential signaling mechanisms responsible for its vasodilatory action. Interestingly, the vasorelaxant effect of HTZZ was diminished by Ruthenium Red (50 μmol·L$^{-1}$), an inhibitor of RyRs (Figs. 5A, 5D) and Verapamil (1 μmol·L$^{-1}$), a blocker of LTCCs (Figs. 5B, 5E), whereas neither blockers of other signaling pathways nor inhibitors of other ion channels exhibited such effects (Fig. S7). Additionally, the vasorelaxant effect of HTZZ was significantly suppressed in calcium-free PSS solution (Figs. 5C, 5F). These results indicate that HTZZ induces vasodilation through inhibition of LTCCs and RyRs.

**Table 3** KEGG enrichment analysis of top 3 MCODE genes function clusters

| Cluster | KEGG terms | −log$_{10}$ *P* |
|---|---|---|
| Cluster 1 | Motor proteins | 6.00 |
| Cluster 1 | Cell cycle | 3.23 |
| Cluster 1 | Platinum drug resistance | 1.03 |
| Cluster 2 | Complement and coagulation cascades | 9.28 |
| Cluster 2 | Cholesterol metabolism | 6.35 |
| Cluster 2 | Platelet activation | 3.27 |
| Cluster 3 | MAPK signaling pathway | 16.80 |
| Cluster 3 | Arrhythmogenic right ventricular cardiomyopathy | 12.01 |
| Cluster 3 | Cardiac muscle contraction | 11.68 |

### *3.8. HTZZ inhibits the activity of L-type calcium channels and RyRs, as well as the expression of L-type calcium channels*

High $K^+$ (60 mmol·L$^{-1}$) induced membrane depolarization in VSMCs, triggering extracellular $Ca^{2+}$ influx through Voltage-Dependent Calcium Channels (VDCCs). To investigate HTZZ's effect on high $K^+$-induced $Ca^{2+}$ influx, we measured cytosolic [$Ca^{2+}$]i in A10 cells using Fluo-4/AM fluorescent probes. The results demonstrated that treatment with both HTZZ (2 mg·mL$^{-1}$) and verapamil (1 μmol·L$^{-1}$) for 20 minutes significantly reduced intracellular calcium levels ([$Ca^{2+}$]i) following $CaCl_2$ (1.8 mmol·L$^{-1}$) administration (Figs.6A, 6B). Consistent with the fluorescence analysis results, flow cytometry analysis similarly demonstrated that both HTZZ (2 mg·mL$^{-1}$) and verapamil (1 μmol·L$^{-1}$) treatment for

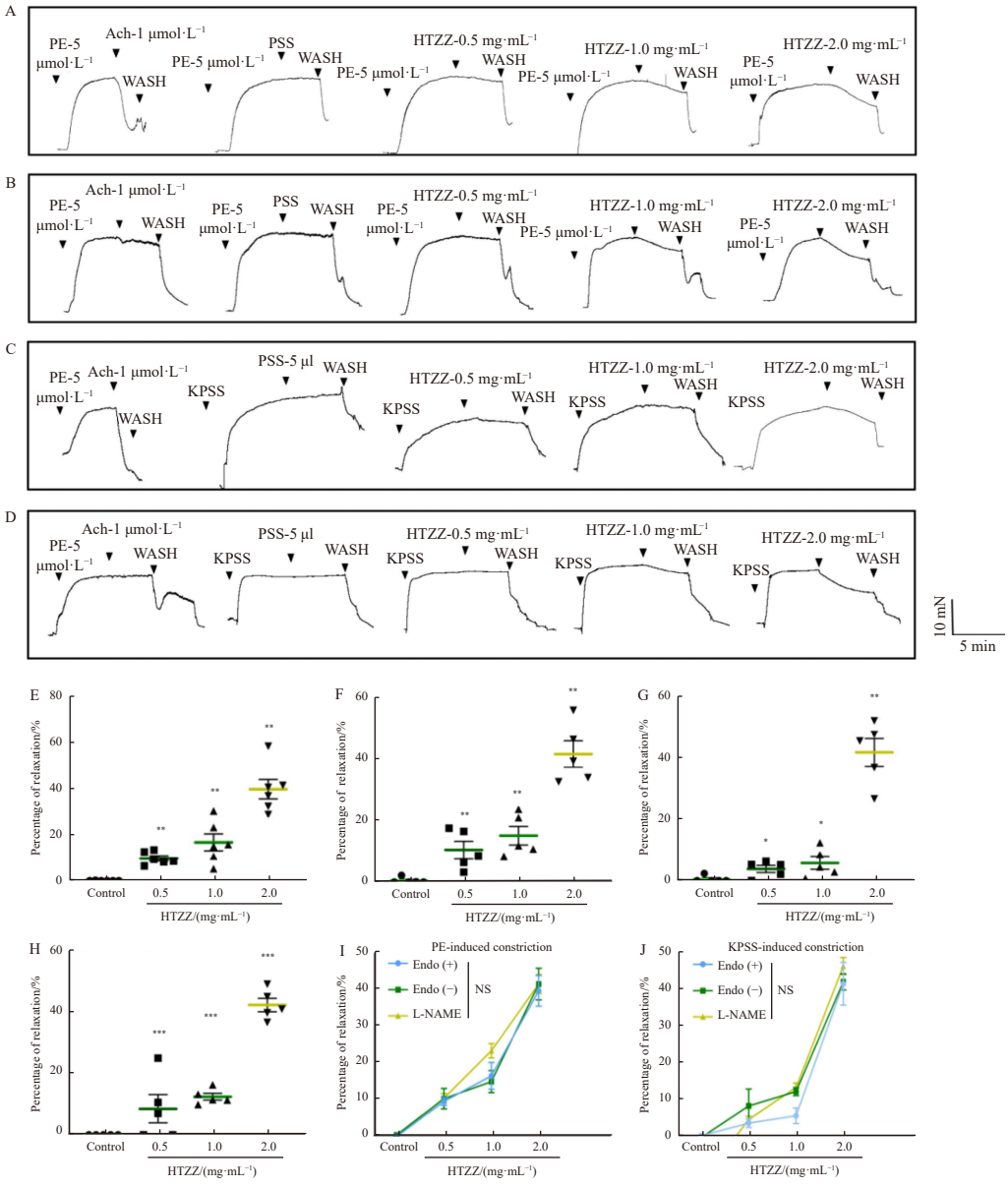


**Fig. 4** HTZZ exhibits vasodilatory effects on PE or KPSS-induced vasoconstriction in a dose-dependent but not endothelium-dependent manner. (A) Representative tension recording image of HTZZ (0.5, 1, 2 mg·mL$^{-1}$) on vasodilation of endothelium-intact vascular rings preconstricted by PE. (B) Representative tension recording image of HTZZ (0.5, 1, 2 mg·mL$^{-1}$) on vasodilation of endothelium-denuded vascular rings preconstricted by PE. (C) Representative tension recording image of HTZZ (0.5, 1, 2 mg·mL$^{-1}$) on vasodilation of endothelium-intact vascular rings preconstricted by KPSS. (D) Representative tension recording image of HTZZ (0.5, 1, 2 mg·mL$^{-1}$) on vasodilation of endothelium-denuded vascular rings preconstricted by KPSS. (E) Quantitative analysis of the relaxation response of endothelium-intact vascular rings to varying concentrations of HTZZ (0.5, 1, 2 mg·mL$^{-1}$) after preconstriction with PE. ($n$ = 5) (F) Quantitative analysis of the relaxation response of endothelium-denuded vascular rings to varying concentrations of HTZZ (0.5, 1, 2 mg·mL$^{-1}$) after preconstriction with PE. ($n$ = 5) (G) Quantitative analysis of the relaxation response of endothelium-intact vascular rings to varying concentrations of HTZZ (0.5, 1, 2 mg·mL$^{-1}$) after preconstriction with KPSS ($n$ = 5). (H) Quantitative analysis of the relaxation response of endothelium-denuded vascular rings to varying concentrations of HTZZ (0.5, 1, 2 mg·mL$^{-1}$) after preconstriction with KPSS ($n$ = 5). (I) Concentration-response curves of the vasodilative effect of HTZZ on endothelium-intact, endothelium-denuded and L-NAME-pretreated vascular rings after preconstriction with PE. $n$ = 5 or 6 (J) Concentration-response curves of the vasodilative effect of HTZZ on endothelium-intact, endothelium-denuded and L-NAME-pretreated vascular rings after preconstriction with KPSS. $n$ = 5 or 6. Data are presented as mean ± SEM. $^{***}P < 0.001$ *vs* Control, $^{**}P < 0.01$ *vs* Control, $^{*}P < 0.05$ *vs* Control. $^{###}P < 0.001$ *vs* Model, $^{##}P < 0.01$ *vs* Model, $^{#}P < 0.05$ *vs* Model.

20 minutes significantly reduced intracellular calcium levels ([$Ca^{2+}$]i) following $CaCl_2$ (1.8 mmol·L$^{-1}$) administration (Figs. 6C, 6D).

To further investigate the mechanism of HTZZ, we employed whole-cell patch-clamp techniques to evaluate its effects on L-type calcium channel activity by measuring the corresponding currents in A10 cells. Whole-cell patch-clamp recordings showed that 20-min exposure to HTZZ (2 mg·mL$^{-1}$) significantly decreased L-type calcium channel current densities in A10 cells, indicating potent inhibition of L-type calcium channel activity (Figs. 6E, 6F). To investigate HTZZ's effects on ryanodine receptors (RyRs) activity, we performed $^{3}$H-ryanodine binding assays. The results showed that treatment with both HTZZ (2 mg·mL$^{-1}$) and ruthenium red (10 μmol·L$^{-1}$) for 20 min significantly reduced RyR activity in A10 cells (Fig. 6G).

Finally, to determine whether HTZZ affects L-type calcium channel protein expression and phosphorylation, we examined its effects after different treatment durations. The results showed that short-term HTZZ (2 mg·mL$^{-1}$) treatment (15, 30, and 60 min) did not alter L-type calcium channel protein levels or phosphorylation status (Fig. 6H). However, prolonged exposure (24 h) significantly suppressed both L-type calcium channel protein and mRNA expression (Figs. 6I, 6J).

## 4. Discussion

The traditional Chinese medicine compound preparation HTZZ is mainly prescribed during the recovery phase and for se-

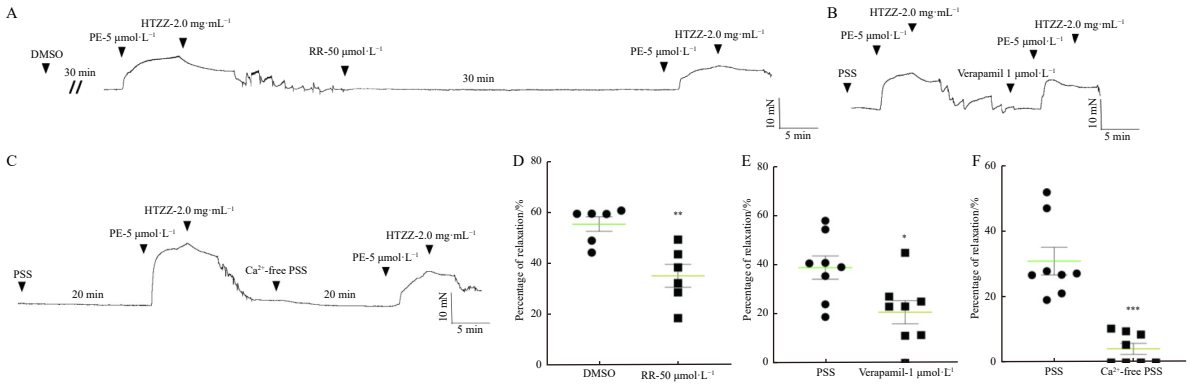


**Fig. 5** HTZZ triggers vasorelaxation by suppressing the activity of RyRs and LTCCs. (A) Representative tension recording image of HTZZ (2 mg·mL$^{-1}$) on vasodilation of endothelium-intact vascular rings preconstricted by Ruthenium Red for 30 min. (B) Representative tension recording image of HTZZ (2 mg·mL$^{-1}$) on vasodilation of endothelium-intact vascular rings preconstricted by Verapamil for 5 min. (C) Representative tension recording image of HTZZ (2 mg·mL$^{-1}$) on vasodilation of endothelium-intact vascular rings preconstricted by calcium-free PSS solution for 20 min. (D–F) Quantitative analysis of the contractile response of endothelium-intact vascular rings. $^{**}P < 0.01$ *vs* DMSO ($n = 8$), $^{*}P < 0.05$ *vs* PSS ($n = 8$), $^{***}P < 0.001$ *vs* PSS ($n = 8$). Data are presented as mean ± SEM.

quelae of stroke in clinical practice [28]. Recent studies have revealed its diverse pharmacological activities, including lipid regulation, promotion of angiogenesis and neuroregeneration, anticoagulation, and immunomodulation [29-31]. These properties have broadened its clinical applications, including in CHD-associated angina pectoris. A randomized, double-blind, placebo-controlled clinical trial demonstrated that 4 weeks of HTZZ intervention significantly reduced the frequency and duration of angina episodes in patients with stable angina, confirming its clinical anti-angina effect. Consistent with these clinical observations, our animal experiments further verified the anti-angina effect of HTZZ in a pituitrin-induced acute myocardial ischemia mouse model and demonstrated its ability to improve vascular elasticity and vasodilatory function in SHRs.

In this study, an acute myocardial ischemia model was established in mice using pituitrin. Pituitrin is rich in vasopressin, which promotes renal water reabsorption and induces potent vasoconstriction [28]. Although this model cannot fully replicate the pathological process of vascular stenosis/spasm caused by atherosclerosis in human CHD [29, 30], it effectively simulates an important cause of myocardial ischemia, namely abnormal vascular contraction induced by various factors [31]. Therefore, it is commonly employed in the construction of animal models of acute myocardial ischemia [32, 33]. Consistent with the clinical observations, HTZZ effectively alleviated angina-like symptoms in this model, suggesting potential therapeutic value. Owing to the limitations of this animal model, the therapeutic effect of HTZZ on atherosclerosis-related myocardial ischemia requires further validation in models that more closely resemble human pathology, such as ApoE$^{-/-}$ mice.

Abnormal vascular tension is a key contributor to angina in CHD, and promoting coronary vasodilation is a crucial therapeutic strategy [34]. The elevated blood pressure observed in SHRs is primarily driven by central nervous system dysfunction, especially within the limbic-hypothalamic axis [35]. This neuroendocrine imbalance leads to hyperactivation of the sympathetic nervous system and hormonal axes (ACTH and TSH), resulting in vascular endothelial dysfunction, smooth muscle remodeling, and increased vascular tone [36, 37]. Notably, SHRs also exhibit an intrinsic defect in vascular smooth muscle cells (VSMCs), characterized by elevated calcium sensitivity, which further impairs vasodilation [38]. Given these features, the SHR model was used to evaluate the vasoprotective effects of HTZZ and to explore its mechanisms of action. Our findings indicate that HTZZ significantly improves vascular elasticity and vasodilatory function in SHRs.

To further investigate the vasodilatory potential of HTZZ, we examined its effects on vascular tension in ex vivo mesenteric arterial ring models. HTZZ effectively inhibited vasoconstriction induced by PE and high potassium and relaxed pre-contracted vessels. Importantly, this vasodilatory effect was not attenuated by endothelial denudation or pretreatment with L-NAME, indicating that HTZZ acts primarily through VSMCs rather than through the endothelium.

Vascular smooth muscle contraction is primarily regulated by various ion channels—including voltage-gated calcium channels (VGCCs), voltage-gated potassium channels (KVs), large-conductance calcium-activated potassium channels (BKCa), inward rectifier potassium channels (KIRs), ATP-sensitive potassium channels (KATP), ryanodine receptors (RyRs), inositol trisphosphate receptors (IP3Rs), and transient receptor potential (TRP) channels—as well as by membrane receptors and intracellular signaling pathways [39, 40]. Our study showed that verapamil, a VGCC blocker, and ryanodine, an RyR inhibitor, significantly attenuated the vasodilatory effect of HTZZ, whereas inhibitors of other pathways had no effect. Furthermore, HTZZ reduced calcium influx and suppressed LTCC and RyR activity in A10 VSMCs. These findings support the hypothesis that HTZZ induces vasodilation primarily by inhibiting LTCC- and RyR-mediated calcium signaling in VSMCs.

This study has two limitations. First, in the clinical study, the treatment duration was limited to 4 weeks, focusing on the short-term efficacy of HTZZ in angina pectoris. Consequently, long-term outcomes, such as angina recurrence rates at 3 or 6 months, were not assessed. Second, only 12 components of HTZZ were identified in the quality control, making it difficult to predict the active ingredients and therapeutic targets of HTZZ through network pharmacology analysis. Additionally, although the present study identified some chemical constituents of HTZZ, it did not determine the primary components responsible for regulating LTCC or RyR, nor did it explore potential synergistic effects among the components.

In summary, this study employed three complementary models—an acute myocardial ischemia model, an *ex vivo* mesenteric arterial ring assay, and the SHR model—to investigate the therapeutic potential of HTZZ in CHD with angina pectoris. Our results demonstrate that HTZZ alleviates angina by improving vascular diastolic function, primarily through inhibition of LTCC and RyR activity and suppression of LTCC expression. As a traditional Chinese patent medicine, HTZZ contains a complex mixture of bioactive compounds, exhibiting multi-component, multi-target, and multi-pathway effects. Further in-depth studies are warranted to fully elucidate its mechanisms of action and support its clinical application in cardiovascular diseases.

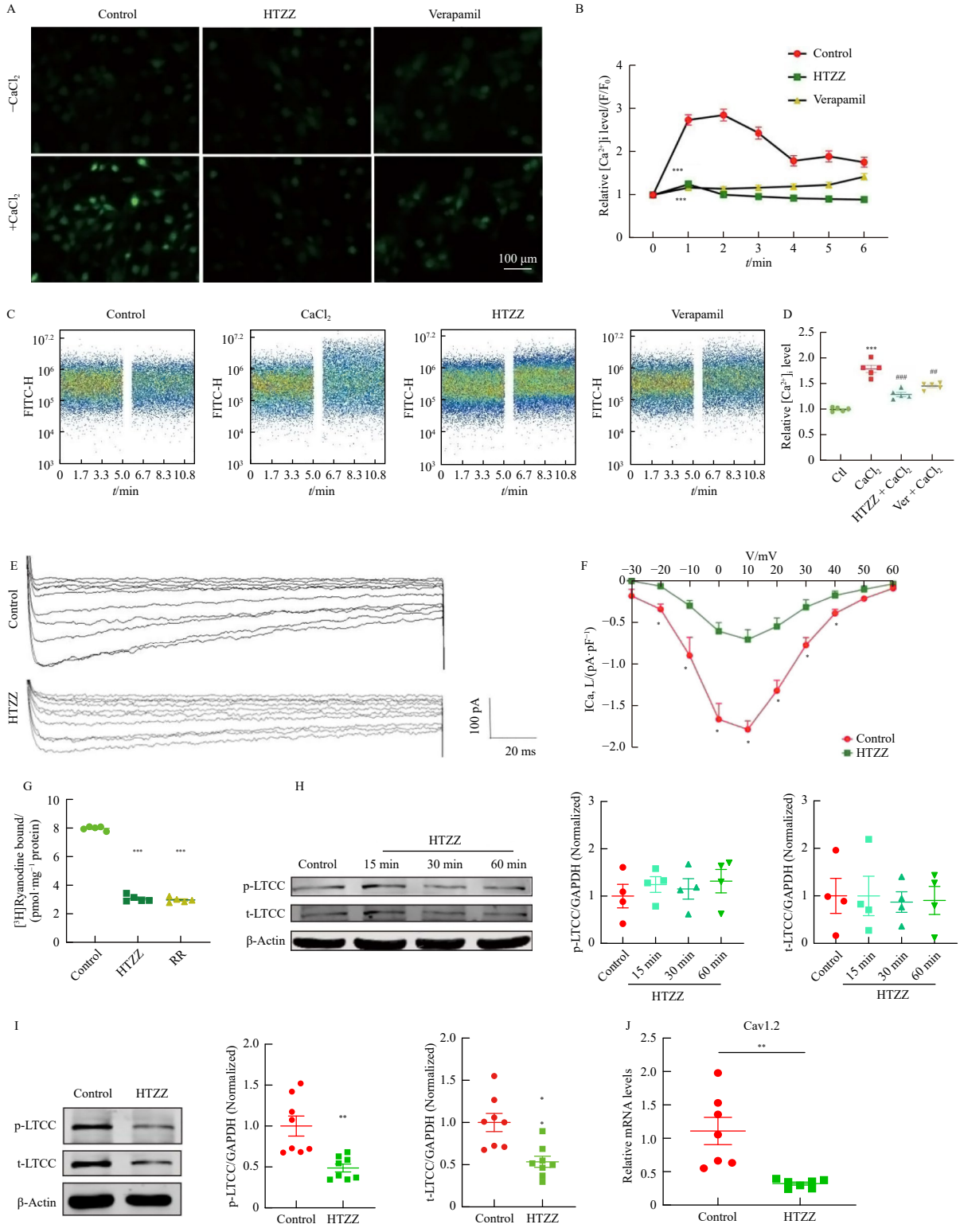


**Fig. 6** Effects of HTZZ on LTCCs and RyRs, and on LTCC Expression. (A) The cytosolic [$Ca^{2+}$]i of A10 cells was measured by Fluo-4/AM fluorescent probe and fluorescence microscope.(B) Graph of the data from Fig. 7A.$^{***}P < 0.001$ *vs* control($n$ = 40–60). (C) The cytosolic [$Ca^{2+}$]i of A10 cells was measured by Fluo-4/AM fluorescent probe and flow cytometer. (D) Graph of the data from Fig.7C. $^{***}P < 0.001$ *vs* Control, $^{\#\#\#}P < 0.001$ *vs* $CaCl_2$, $^{\#\#}P < 0.01$ *vs* $CaCl_2$.(E) Representative traces of L-type VDCC currents.(F) Current density-voltage ($I_{Ca,L}$-V) plots for the L-type VDCC currents following treatment with 2 mg·$mL^{-1}$ of HTZZ for 20 minutes. $^{*}P < 0.05$ *vs* the Ctl group ($n$ = 7). $n$, number of independent cells. (G) The effect of HTZZ on the activity of the Ryanodine Receptors (RyRs). $^{***}P < 0.001$ *vs* Control ($n$ = 5). (H) Representative Western blot images and quantification of protein levels of t-LTCC and p-LTCC in A10 cells at 15, 30 and 60 minutes after HTZZ administration. $^{*}P < 0.05$ *vs* Control ($n$ = 4). (I) Representative Western blot images and quantification of protein levels of t-LTCC and p-LTCC in A10 cells at 24 hours after HTZZ administration. $^{*}P < 0.05$ *vs* Control ($n$ = 7). (J) The mRNA of LTCC in A10 cells at 24 hours after HTZZ administration.$^{**}P < 0.01$ *vs* Control ($n$ = 6). Data are presented as mean ± SEM.

## Fundings

This study was supported by Noncommunicable Chronic Diseases-National Science and Technology Major Project (No. 2024ZD0537900), the National Multidisciplinary Cross-innovation Team Project in Traditional Chinese Medicine(No. ZYYCXTD-D-202407), the National Natural Science Foundation of China (No. 82330011) and the China Postdoctoral Science Foundation

(No. 2023MD744216).

## Supporting information

Supporting information for this work can be obtained by contacting the corresponding authors *via* E-mail.

## Declaration of competing interests

Guangzhou Baiyunshan Qixing Pharmaceutical Co. Ltd. donated the study drugs, including Huatuo Zaizao Pills and the placebo for the clinical research, but had no role in the data acquisition, statistical analysis and interpretation of the results.

Ms. Na Ning is the employee of Guangzhou Baiyunshan Qixing Pharmaceutical Co. Ltd. The authors declare that they have no known competing financial interests or personal relationships that could have appeared to influence the work reported in this paper. Dr. Nannan Wang is the employee of Guangzhou Baiyunshan Zhongyi Pharmaceutical Co. Ltd.

## References


1 Atwood J. Management of acute coronary syndrome. *Emerg Med Clin North Am*. 2022;40:693-706. https://doi.org/10.1016/j.emc.2022.06.008.
2 Picard F, Sayah N, Spagnoli V, et al. Vasospastic angina: a literature review of current evidence. *Arch Cardiovasc Dis*. 2019;112:44-55. https://doi.org/10.1016/j.acvd.2018.08.002.
3 Minhas A, Cubero Salazar I, Kazzi B, et al. Sex-specific plaque signature: uniqueness of atherosclerosis in women. *Curr Cardiol Rep*. 2021;23(7):84. https://doi.org/10.1007/s11886-021-01513-3.
4 Kiaie N, Gorabi AM, Penson PE, et al. A new approach to the diagnosis and treatment of atherosclerosis: the era of the liposome. *Drug Discov Today*. 2020;25:58-72. https://doi.org/10.1016/j.drudis.2019.09.005.
5 Al-Lamee RK. Angina pectoris 2023: with and without obstructive coronary artery disease: epidemiology, diagnosis, prognosis, and treatment. *Vascul Pharmacol*. 2024;155:107285. https://doi.org/10.1016/j.vph.2024.107285.
6 Senderovic A, Galijasevic S. The role of inducible nitric oxide synthase in assessing the functional level of coronary artery lesions in chronic coronary syndrome. *Cardiol Res*. 2024;15:330-339. https://doi.org/10.14740/cr1700.
7 Damani DN, Roongsritong C. Zero coronary artery calcification: a promising value in acute chest pain evaluation. *Cureus*. 2025;17:e78365. https://doi.org/10.7759/cureus.78365.
8 Baghina RM, Crisan S, Luca S, et al. Association between inflammation and new-onset atrial fibrillation in acute coronary syndromes. *J Clin Med*. 2024;13(17):5088. https://doi.org/10.3390/jcm13175088.
9 Fan L, Wang H, Kassab GS, et al. Review of cardiac-coronary interaction and insights from mathematical modeling. *WIREs Mech Dis*. 2024;16(3):e1642. https://doi.org/10.1002/wsbm.1642.
10 Ortega FB, Lavie CJ, Blair SN. Obesity and cardiovascular disease. *Circ Res*. 2016;118(11):1752-1770. https://doi.org/10.1161/CIRCRESAHA.115.306883.
11 Ulbricht TL, Southgate DA. Coronary heart disease: seven dietary factors. *Lancet*. 1991;338:985-992. https://doi.org/10.1016/0140-6736(91)91846-m.
12 Kuga T, Shimokawa H, Hirakawa Y, et al. Increased expression of L-type calcium channels in vascular smooth muscle cells at spastic site in a porcine model of coronary artery spasm. *J Cardiovasc Pharmacol*. 2000;35(5):822-828. https://doi.org/10.1097/00005344-200005000-00021.
13 Avila-Medina J, Calderon-Sanchez E, Gonzalez-Rodriguez P, et al. Orai1 and TRPC1 proteins co-localize with CaV1. *2 channels to form a signal complex in vascular smooth muscle cells. J Biol Chem*. 2016;291(40):21148-21159. https://doi.org/10.1074/jbc.M116.742171.
14 Trebak M. STIM/Orai signalling complexes in vascular smooth muscle. *J Physiol*. 2012;590(17):4201-4208. https://doi.org/10.1113/jphysiol.2012.233353.
15 Woll KA, Van Petegem F. Calcium-release channels: structure and function of $IP_3$ receptors and ryanodine receptors. *Physiol Rev*. 2022;102(1):209-268. https://doi.org/10.1152/physrev.00033.2020.
16 Kochegarov AA. Pharmacological modulators of voltage-gated calcium channels and their therapeutical application. *Cell Calcium*. 2003;33(3):145-162. https://doi.org/10.1016/s0143-4160(02)00239-7.
17 Large WA. Receptor-operated $Ca^{2+}$-permeable nonselective cation channels in vascular smooth muscle: a physiologic perspective. *J Cardiovasc Electrophysiol*. 2002;13(5):493-501. https://doi.org/10.1046/j.1540-8167.2002.00493.x.
18 Hidalgo C, Donoso P, Carrasco MA. The ryanodine receptors $Ca^{2+}$ release channels: cellular redox sensors? *IUBMB Life*. 2005;57(4-5):315-322. https://doi.org/10.1080/15216540500092328
19 Rokolya A, Ahn HY, Moreland S, et al. A hypothesis for the mechanism of receptor and G-protein-dependent enhancement of vascular smooth muscle myofilament $Ca^{2+}$ sensitivity. *Can J Physiol Pharmacol*. 1994;72(11):1420-1426. https://doi.org/10.1139/y94-205.
20 Khalil RA. Regulation of vascular smooth muscle function. San Rafael (CA): Morgan & Claypool Life Sciences; 2010.
21 Zhang J, Zhang HL, Xu XR, et al. Targeting PBK with small-molecule 1-O-acetyl-4R,6S-britannilactone for the treatment of neuroinflammation. *Proc Natl Acad Sci U S A*. 2025;122(29):e2502593122. https://doi.org/10.1073/pnas.2502593122.
22 Zhang J, Zhang M, Huo XK, et al. Macrophage inactivation by small molecule wedelolactone *via* targeting sEH for the treatment of LPS-induced acute lung injury. *ACS Cent Sci*. 2023;9(3):440-456. https://doi.org/10.1021/acscentsci.2c01424.
23 Zhang J, Zhang M, Zhu QM, et al. Allosteric regulation of Keap1 by 8β-hydroxy-α-cyclocostunolide for the treatment of acute lung injury. *Acta Pharm Sin B*. 2024;14(9):4174-4178. https://doi.org/10.1016/j.apsb.2024.06.025.
24 Zhang J, Luan ZL, Huo XK, et al. Direct targeting of sEH with alisol B alleviated the apoptosis, inflammation, and oxidative stress in cisplatin-induced acute kidney injury. *Int J Biol Sci*. 2023;19(1):294-310. https://doi.org/10.7150/ijbs.78097.
25 Sun CP, Zhou JJ, Yu ZL, et al. Kurarinone alleviated Parkinson's disease *via* stabilization of epoxyeicosatrienoic acids in animal model. *Proc Natl Acad Sci U S A*. 2022;119(9):e2118818119. https://doi.org/10.1073/pnas.2118818119.
26 Jiang S, Yu LJ, Yang H, et al. A study on inhibition of the Aβ(1-42)-induced inflammatory response by the Huatuo Zaizao pill through the NF-κB signaling pathway. *Arch Med Sci*. 2020;19(4):1136-1144. https://doi.org/10.5114/aoms.2020.99427.
27 Duan S, Wang T, Zhang J, et al. Huatuo Zaizao pill promotes functional recovery and neurogenesis after cerebral ischemia-reperfusion in rats. *BMC Complement Altern Med*. 2017;17(1):19. https://doi.org/10.1186/s12906-016-1516-z.
28 Yang S, Zhao Y, Cheng X, et al. Buxu Tongyu Granule alleviates myocardial ischemia by activating vascular smooth muscle cell soluble guanylate cyclase to inhibit abnormal vasomotion. *Engineering*. 2024;38:133-143. https://doi.org/10.1016/j.eng.2023.06.009.
29 Homayounieh F, Yan P, Digumarthy SR, et al. Prediction of coronary calcification and stenosis: role of radiomics from low-dose CT. *Acad Radiol*. 2021;28(7):972-979. https://doi.org/10.1016/j.acra.2020.09.021.
30 Okumura K, Yasue H, Matsuyama K, et al. A study on coronary hemodynamics during acetylcholine-induced coronary spasm in patients with variant angina: endothelium-dependent dilation in the resistance vessels. *J Am Coll Cardiol*. 1992;19(7):1426-1434. https://doi.org/10.1016/0735-1097(92)90598-h.
31 Yasue H, Kugiyama K. Coronary spasm: clinical features and pathogenesis. *Intern Med*. 1997;36(11):760-765. https://doi.org/10.2169/internalmedicine.36.760.
32 Brown CH. Magnocellular neurons and posterior pituitary function. *Compr Physiol*. 2016;6(4):1701-1741. https://doi.org/10.1002/cphy.c150053.
33 Lin S, Chu J, Zhang L, et al. Protective effects of Shexiang Tongxin Dropping Pill on pituitrin-induced acute myocardial ischemia in rats. *Mol Med Rep*. 2017;16(3):3125-3132. https://doi.org/10.3892/mmr.2017.6963.
34 Yasue H, Nakagawa H, Itoh T, et al. Coronary artery spasm: clinical features, diagnosis, pathogenesis, and treatment. *J Cardiol*. 2008;51(1):2-17. https://doi.org/10.1016/j.jjcc.2008.01.001.
35 Prieto I, Segarra AB, de Gasparo M, et al. Divergent profile between hypothalamic and plasmatic aminopeptidase activities in WKY and SHR: influence of β-adrenergic blockade. *Life Sci*. 2018;192:9-17. https://doi.org/10.1016/j.lfs.2017.11.022.
36 Fujiwara T. A study of TSH-synthesis of spontaneous hypertensive rats by electron microscopic morphometry and autoradiography. *Cell Tissue Res*. 1979;201(3):467-477. https://doi.org/10.1007/BF00237005.
37 Oparil S, Yang RH, Jin HK, et al. Central mechanisms of hypertension. *Am J Hypertens*. 1989;2(6 Pt 1):477-485. https://doi.org/10.1093/ajh/2.6.477
38 Pegram BL, Ljung B. Neuroeffector function of isolated portal vein from spontaneously hypertensive and Wistar-Kyoto rats: dependence on external calcium concentration. *Blood Vessels*. 1981;18(3):89-99. https://doi.org/10.1159/000158341.
39 Tykocki NR, Boerman EM, Jackson WF. Smooth muscle ion channels and regulation of vascular tone in resistance arteries and arterioles. *Compr Physiol*. 2017;7(2):485-581. https://doi.org/10.1002/cphy.c160011.
40 Zhao Y, Zhu J, Liang H, et al. Kang le xin reduces blood pressure through inducing endothelial-dependent vasodilation by activating the AMPK-eNOS pathway. *Front Pharmacol*. 2020;10:1548. https://doi.org/10.3389/fphar.2019.01548.